

Unconventional Coherence Peak in Cuprate Superconductors

Zheng Li,^{1,2,*} Chao Mu,^{1,2} Pengfei Li,^{1,2} Wei Wu,¹ Jiangping Hu,^{1,3} Tao Xiang,^{1,2} Kun Jiang,^{1,2,†} and Jianlin Luo^{1,2,‡}

¹*Beijing National Laboratory for Condensed Matter Physics and Institute of Physics, Chinese Academy of Sciences, Beijing 100190, China*

²*School of Physical Sciences, University of Chinese Academy of Sciences, Beijing 100190, China*
³*New Cornerstone Science Laboratory, Beijing 100190, China.*

The Hebel-Slichter coherence peak, observed in the spin-lattice relaxation rate $1/T_1$ just below the critical temperature T_c , serves as a crucial experimental validation of the Bardeen-Cooper-Schrieffer pairing symmetry in conventional superconductors. However, no coherence peak in $1/T_1$ has been observed in unconventional superconductors like cuprates. In this study, an unconventional coherence peak is identified for the first time using nuclear quadrupole resonance on $\text{YBa}_2\text{Cu}_4\text{O}_8$, pointing to a distinctive pairing symmetry. The spin-lattice relaxation rate in nuclear quadrupole resonance and nuclear magnetic resonance with nuclear spin $I > 1/2$ comprises the magnetic relaxation rate $1/T_1^{\text{mag}}$, which probes magnetic fluctuations, and the quadrupole relaxation rate $1/T_1^{\text{quad}}$, which probes charge fluctuations. By utilizing ^{63}Cu and ^{65}Cu isotopes, we successfully distinguish $1/T_1^{\text{mag}}$ and $1/T_1^{\text{quad}}$ of $\text{YBa}_2\text{Cu}_4\text{O}_8$ and reveal the presence of the coherence peak in $1/T_1^{\text{quad}}$ but not in $1/T_1^{\text{mag}}$, in contrast to conventional superconductors. Our finding demonstrates that unconventional superconductors do not exhibit a coherence peak in $1/T_1$ when the relaxation is due to fluctuations of the hyperfine field. Conversely, a coherence peak is expected when the relaxation is caused by electric field gradient fluctuations, due to the different coherence factors between charge and magnetic fluctuations. Our successful measurements of $1/T_1$ for the chains of $\text{YBa}_2\text{Cu}_4\text{O}_8$ suggest that, should the conditions for predominant quadrupole relaxation be satisfied, this phenomenon could provide a novel approach to exploring the unconventional nature of the pairing mechanism in other superconductors.

I. INTRODUCTION

Unconventional superconductors, such as d -wave and s^\pm -wave superconductors, are characterized by a varying sign of the superconducting gap function in momentum space, with their Cooper pairs widely believed to originate from electron-electron correlation rather than electron-phonon coupling[1]. Therefore, unconventional superconductors exhibit distinct physical properties, such as the absence of the Hebel-Slichter coherence peak [2–10]. In conventional superconductors with uniform superconducting gaps, the density of states (DOS) diverges at the gap energy, leading to a huge enhancement of spin-lattice relaxation rate $1/T_1$ just below the critical temperature T_c in nuclear magnetic resonance (NMR) experiment, called the Hebel-Slichter coherence peak[11]. Conversely, this Hebel-Slichter coherence peak is absent in unconventional superconductors[10], such as d -wave cuprate superconductors, where the DOS divergence persists. Consequently, detecting coherence peaks poses a significant challenge for unconventional superconductors. In this work, we reveal a novel unconventional coherence peak in high-temperature cuprate superconductors using nuclear quadrupole resonance (NQR), introducing a distinctive feature of unconventional superconductivity.

The nucleus with the spin $I > 1/2$ is nonspherical and possesses an electric quadrupole moment $Q_{\alpha\beta}$, where α and β are spatial directions x, y, z . This results in the nucleus having an electrostatic energy that varies depending on its orientation within an electric field gradient (EFG) $V_{\alpha\beta} = \frac{\partial^2 V}{\partial \alpha \partial \beta}$ generated by the local potential V from its surrounding environments[12]. Hence, the electrostatic energy splitting between different nucleus spin $|I|$ is utilized in NQR, analogous to how NMR employs the magnetic energy splitting of each spin I under a magnetic field. Furthermore, the electric quadrupole moment is a valuable tool for investigating electric field dynamics, akin to how the magnetic moment is used to study spin dynamics. These tools complement each other in exploring electromagnetic fluctuations in condensed matter[13]. A key dynamic signal is the spin-lattice relaxation rate, which describes how the nuclei arrive at their thermal equilibrium via the process of spin-lattice relaxation and is proportional to the summation of the imaginary part of the dynamical susceptibility. In the conventional s -wave superconducting state, the rate can be expressed as[14]

$$\frac{T_{1N}}{T_{1S}} = -\frac{2}{N_0^2} \int_{\Delta}^{\infty} \left(1 \pm \frac{\Delta^2}{E^2}\right) N_S^2(E) \frac{\partial f(E)}{\partial E} dE \quad (1)$$

where T_{1N} and T_{1S} are the relaxation times in the normal state and the superconducting state, respectively. N_0 is the DOS in the normal state and $N_S(E) = N_0 E / \sqrt{E^2 - \Delta^2}$ for $E > \Delta$ is the DOS in the superconducting state. $f(E)$ is the Fermi distribution function and Δ is the superconducting gap. The sign of the coherence factor $(1 \pm \Delta^2/E^2)$ is contingent on

* lizheng@iphy.ac.cn

† jiangkun@iphy.ac.cn

‡ jlluo@iphy.ac.cn

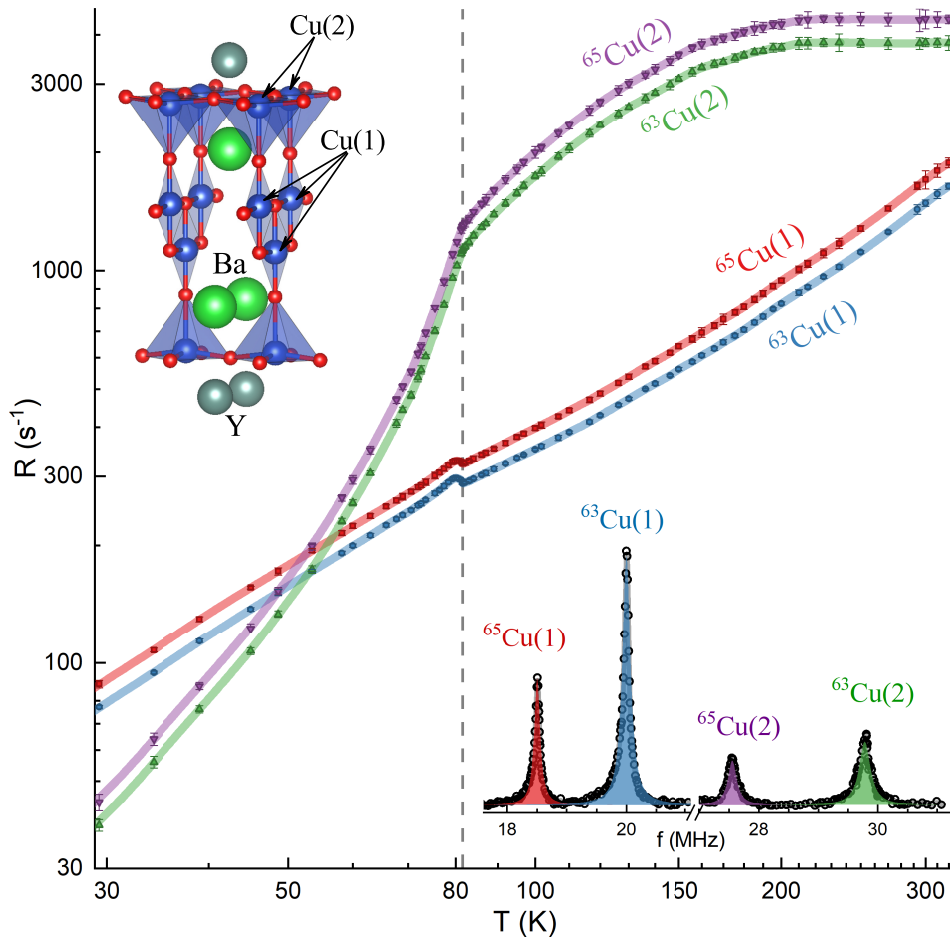


FIG. 1. Temperature dependence of relaxation rate R of $\text{YBa}_2\text{Cu}_4\text{O}_8$. The inset crystal structure indicates the Cu(1) and Cu(2) site. The inset spectrum shows four peaks of ^{63}Cu and ^{65}Cu at the Cu(1) and Cu(2) sites respectively, where R is measured. The dashed line marks the superconducting transition temperature T_c . R of $^{63}\text{Cu}(2)$ (green) and $^{65}\text{Cu}(2)$ (purple) drops below T_c , while R of $^{63}\text{Cu}(1)$ (cyan) and $^{65}\text{Cu}(1)$ (red) increases a little just below T_c and forms a small peak.

the nature of the perturbation causing the transition. Magnetic relaxations, being not time-reversal invariant, have $(1 + \Delta^2/E^2)$ which enhance the divergency of $N_S(E)$ and the magnetic relaxation rate $1/T_1^{\text{mag}}$ exhibits a Hebel-Slichter coherence peak in conventional superconductors[14]. In contrast, quadrupole relaxations, being time-reversal invariant, have $(1 - \Delta^2/E^2)$ which compensate for the divergency of $N_S(E)$ and the quadrupole relaxation rate $1/T_1^{\text{quad}}$ drops rapidly below T_c in conventional superconductors[15, 16]. In unconventional superconductors, $1/T_1^{\text{mag}}$ drops or decreases gradually below T_c , without a coherence peak being observed[2]. These phenomena contradict the logarithmic divergency of $N_S(E)$ in cuprate superconductors[17]. Additionally, the cuprate superconductor gap sign varies in momentum space, significantly impacting the coherence factor and potentially leading to a shift of the coherence peak to $1/T_1^{\text{quad}}$.

II. RESULT

Whether a coherence peak is present in $1/T_1^{\text{quad}}$ motivated us to perform NQR on two isotopes ^{63}Cu and ^{65}Cu in oxygen-stoichiometric and underdoped $\text{YBa}_2\text{Cu}_4\text{O}_8$. This compound is an unconventional superconductor with a transition temperature $T_c = 81.5$ K[18], as confirmed by the temperature-dependent magnetization measurement in Fig. 6. As previously mentioned, NQR is particularly sensitive to the local chemical environment and can distinguish between Cu atoms situated in distinct positions. $\text{YBa}_2\text{Cu}_4\text{O}_8$ contains two Cu sites, namely, the chain Cu(1) and the planar Cu(2) (depicted in the upper inset in Fig. 1), offering a unique avenue to probe $1/T_1^{\text{mag}}$ and $1/T_1^{\text{quad}}$ and explore the coherence peak. The Cu(1) and Cu(2) sites have different EFG strengths, resulting in different resonance frequencies as shown in the spectra inserted in Fig. 1. Additionally,

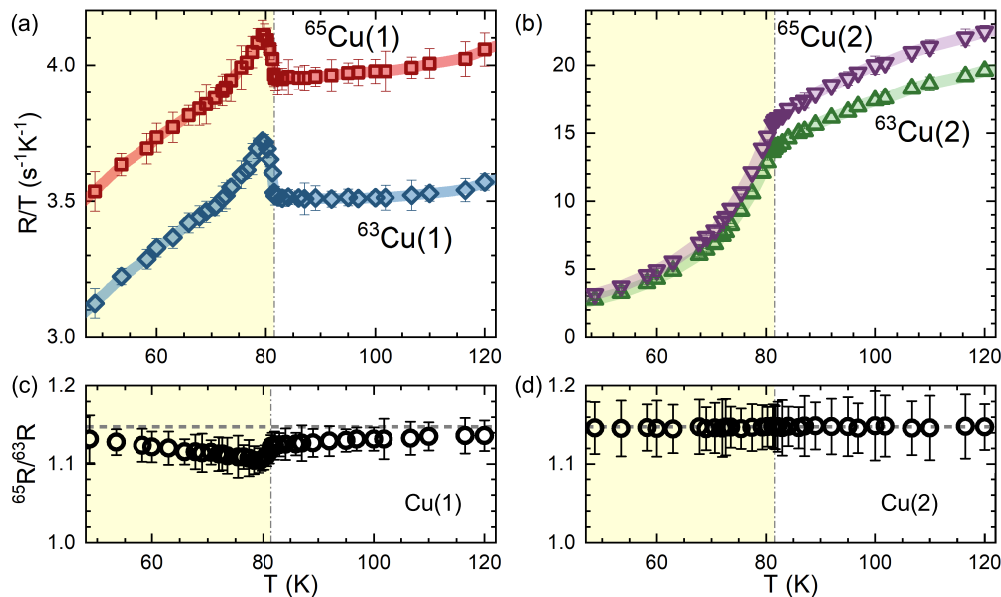


FIG. 2. Temperature dependence of spin-lattice relaxation rates and their ratio of YBa₂Cu₄O₈ around T_c . The superconducting state is marked in yellow. Spin-lattice relaxation rates of ^{65}Cu and ^{63}Cu at the (a) Cu(1) site (cyan and red) and (b) Cu(2) site (purple and green), respectively. A coherence peak can be identified below T_c at the Cu(1) site. (c),(d) Spin-lattice relaxation rate ratios of ^{65}Cu to ^{63}Cu at Cu(1) and Cu(2) sites, respectively. The dashed lines mark the value of $(^{65}\gamma/^{63}\gamma)^2 = 1.1477$, where there is only magnetic relaxation. Deviation from the dashed line indicates quadrupole relaxation emerges below T_c at the Cu(1) site.

the distinct EFG tensors of Cu(1) and Cu(2) influence their electric dynamic behavior, which is discussed later. Two isotopes ^{63}Cu and ^{65}Cu lead to two NQR resonance peaks at each site, for a total of four peaks at both sites, as shown in the lower inset in Fig. 1 for the spectrum at T_c .

The four NQR spin-lattice relaxation rates R corresponding to the four peaks are measured and plotted in Fig. 1. For the planar Cu(2), the R of $^{63}\text{Cu}(2)$ and $^{65}\text{Cu}(2)$ (green and purple lines, respectively) drop due to the reduction in DOS caused by the superconducting gap below T_c , with noticeable kink behaviors observed at T_c . The R of Cu(2) above T_c keeps increasing and saturates around 200 K[19]. These data are consistent with previous reports in the whole temperature range[4, 6] and similar to YBa₂Cu₃O₇[5]. On the other hand, the R of $^{63}\text{Cu}(1)$ and $^{65}\text{Cu}(1)$ (cyan and red lines, respectively) decrease with temperature decreasing above T_c , resembling the behavior of a conventional metal. Notably, the R of Cu(1) exhibits a slight increase just below T_c , followed by a decrease at lower temperatures. These distinctive characteristics are highly unusual, suggesting a coherence peak akin to that observed in conventional superconductors.

Let us focus our attention on the superconducting transition and eliminate the linear temperature term in the metal by drawing R/T around T_c in Figs. 2(a) and 2(b). Both R/T of ^{63}Cu and ^{65}Cu at the Cu(1) site exhibit a coherence peak just below T_c , whereas R/T of the Cu(2) site commences a quite steep descent below

T_c . The distinct temperature-dependence behaviors of Cu(1) and Cu(2) are attributed to their different EFG. R can be expressed as a sum of magnetic relaxation rate $1/T_1^{\text{mag}}$ and quadrupole relaxation rate $1/T_1^{\text{quad}}$, $R = 3/T_1^{\text{mag}} + 1/T_1^{\text{quad}}$ for $I = 3/2$ NQR experiment[20]. Theoretically, the nuclear spin Hamiltonian of the interaction between quadrupole moment Q and EFG can be written as[12]

$$\mathcal{H}_Q = \frac{h\nu_Q}{6} \left[(3I_z^2 - I^2) + \frac{\eta}{2}(I_+^2 + I_-^2) \right] \quad (2)$$

where ν_Q is the quadrupole resonance frequency along the principal axis, $h\nu_Q = 3eQV_{zz}/2I(2I - 1)$. $\eta = (V_{xx} - V_{yy})/V_{zz}$ is an asymmetry parameter of the EFG, where V_{xx} , V_{yy} , and V_{zz} are the EFGs along the x , y , and z directions, respectively. Only the terms with I_+ and I_- can flip spins and contribute to $1/T_1^{\text{quad}}$, necessitating a sufficiently large η to measure $1/T_1^{\text{quad}}$. The planar Cu(2) is isotropic with a negligible η [4], resulting in $1/T_1$ of Cu(2) being purely affected by magnetic relaxation and unable to detect EFG fluctuations[2]. Therefore, although there are charge fluctuations in the Cu-O plane detected by planar ^{17}O with $\eta > 0.2$ [21], they cannot be detected by Cu(2)[22]. On the other hand, the chain Cu(1) is anisotropic with $\eta = 0.85$, causing $1/T_1$ of Cu(1) to be affected by both magnetic and quadrupole relaxation. If the coherence peak is due to magnetic relaxation, it should be observed at both Cu(1) and Cu(2) sites. The presence of the coherence peak exclusively at

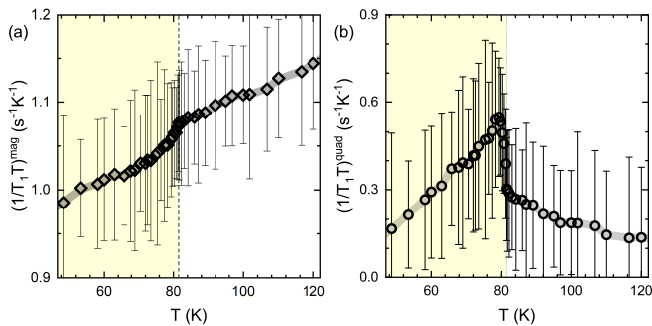


FIG. 3. The relaxation rate of (a) magnetic component $1/(T_1T)^{\text{mag}}$ and (b) the quadrupole component $1/(T_1T)^{\text{quad}}$ at the Cu(1) site. The yellow background indicates the superconducting state. The coherence peak is located at the $1/(T_1T)^{\text{quad}}$ but is absent at the $1/(T_1T)^{\text{mag}}$.

the Cu(1) site suggests its origin from quadrupole relaxation.

$1/T_1^{\text{mag}}$ and $1/T_1^{\text{quad}}$ can be decomposed by utilizing two isotopes $^{63,65}\text{Cu}$, which possess the same spin $I=3/2$ but different gyromagnetic ratios and quadrupole moments[2]. Using isotopes can avoid the influence from form factors and principle axes directions[23], since they occupy the same atom site. The decomposition equations are $3/^{63}T_1^{\text{mag}} = (^{65}R - b \times ^{63}R) / (a - b)$ and $1/^{63}T_1^{\text{quad}} = (a \times ^{63}R - ^{65}R) / (a - b)$, where the quotients $a = (^{65}\gamma/^{63}\gamma)^2 = 1.1477$ and $b = (^{65}Q/^{63}Q)^2 = 0.8562$ are known[24]. Before decomposing, the ratio of $^{65}R/^{63}R$ is calculated to assess the weight of $1/T_1^{\text{mag}}$ and $1/T_1^{\text{quad}}$, shown in Figs. 2(c) and 2(d). $^{65}R/^{63}R$ at the Cu(2) site remains a constant value around the magnetic quotient $a = 1.1477$ for various temperatures, indicating negligible $1/T_1^{\text{quad}}$ and the presence of only $1/T_1^{\text{mag}}$. Conversely, $^{65}R/^{63}R$ at the Cu(1) site deviates from 1.1477

around T_c , suggesting a detectable $1/T_1^{\text{quad}}$ component.

The magnetic and quadrupole relaxations of Cu(1) are decomposed using the relations mentioned above, and the results are illustrated in Figs. 3(a) and 3(b), respectively. The $1/T_1^{\text{mag}}$ depicted in Fig. 3(a) drops below T_c due to the loss of DOS, aligning with the behavior of the R/T at the Cu(2) site where solely magnetic relaxation occurs and $R/T = 3/(T_1T)^{\text{mag}}$. In contrast, the $1/(T_1T)^{\text{quad}}$ displays a prominent coherence peak just below T_c , in sharp contrast to conventional superconductors where the coherence peak is evident in the $1/(T_1T)^{\text{mag}}$ and absent in $1/(T_1T)^{\text{quad}}$. This discrepancy elucidates the absence of a coherence peak at the Cu(2) site, as it is unaffected by quadrupole relaxation. It is noteworthy that the $1/(T_1T)^{\text{quad}}$ is smaller than $1/(T_1T)^{\text{mag}}$, underscoring the higher sensitivity of most nuclei, such as Cu, to magnetic fluctuations in dipolar interaction than to EFG fluctuations in quadrupole interaction. Moreover, in the superconducting state, on lowering the temperature, the quadrupolar relaxation diminishes faster than the magnetic one[22]. Consequently, the coherence peaks in Fig. 2 (a) have historically been inconspicuous and challenging to detect.

There is one thing we need to emphasize: The superfluid density of the system around T_c is dominated by the CuO_2 plane, since the bare transition temperature of the chain is much smaller than the plane owing to the strong fluctuations in one dimension [25–28]. Therefore, although $1/T_1^{\text{quad}}$ is measured at the chains, the peak from $1/T_1^{\text{quad}}$ directly probes the charge dynamics of the CuO_2 plane. To simplify our discussion and arrive at a qualitative understanding, we focus on only the CuO_2 plane and leave the general discussion to the appendix. The newly observed $1/T_1^{\text{quad}}$ peak is proportional to a q -summed charge susceptibility $\chi_\rho(q, E)$ of cuprate superconductivity, underscoring the significance of both long and short wavelengths to $1/T_1^{\text{quad}}$. Theoretically, $1/T_1^{\text{quad}}$ can be written as

$$\frac{1}{T_1^{\text{quad}}} \propto -T \sum_{kq} \left(1 - \frac{\Delta_k \Delta_{k+q}}{E_k^2} \right) F^2(q) \frac{\partial f(E_k)}{\partial E_k} \delta(E_k - E_{k+q}) \quad (3)$$

where the $F(q)$ is the structure factor of the quadrupole interaction. A key aspect of this equation is the coherence factor $(1 - \Delta_k \Delta_{k+q}/E^2)$. For a d -wave superconductor, a prominent momentum q is around $q_0 = (\pi, \pi)$. This q_0 excitation, along with the corresponding coherence factor, has previously resulted in a distinct spin resonance peak in neutron scattering of cuprate superconductors[29]. Similarly, this coherence factor around q_0 gives rise to a sign reversal $\Delta_k \Delta_{k+q_0} < 0$, which cannot counterbalance the divergence from DOS in the superconducting state. Hence, this q_0 may lead

to this unconventional coherence peak in $1/T_1^{\text{quad}}$ upon entering the superconducting transition.

III. DISCUSSION

The unconventional coherence peak identified in the nuclear quadrupole relaxation rate of $\text{YBa}_2\text{Cu}_4\text{O}_8$ complements the relaxation rate pattern depicted in Fig. 4. In conventional superconductors, a Hebel-Slichter coherence peak is typically observed in the magnetic relax-

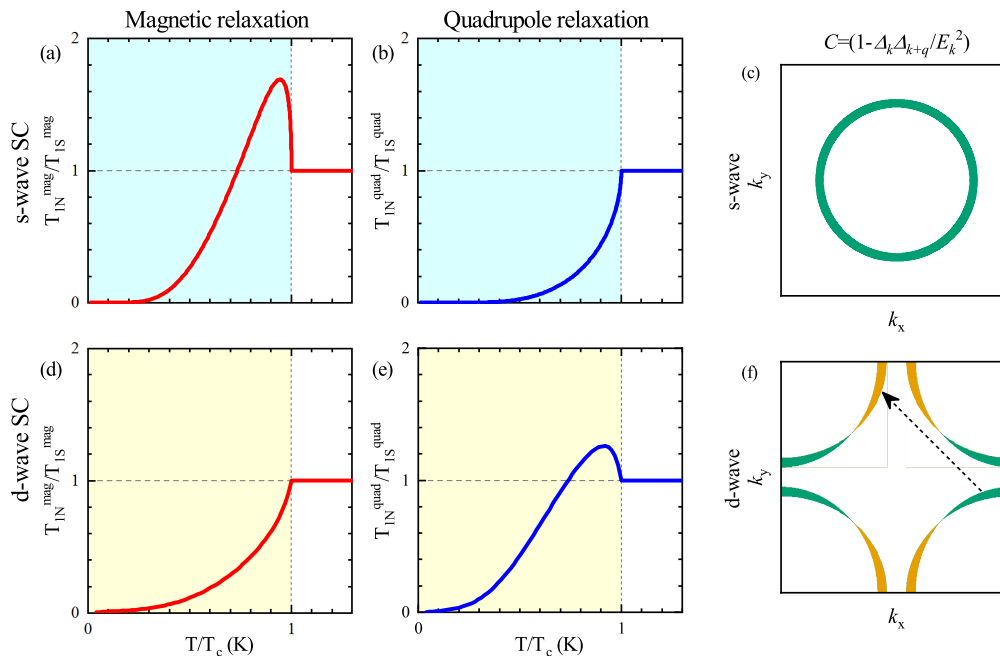


FIG. 4. Schematic diagrams of experimental measured magnetic and quadrupole relaxation rates of conventional and unconventional superconductors. The cyan and yellow backgrounds represent the conventional and unconventional superconducting states, respectively. (a) The magnetic relaxation rate shows a Hebel-Slichter coherence peak just below T_c , while (b) the quadrupole relaxation rate drops rapidly below T_c in conventional superconductors. In unconventional superconductors, (d) the magnetic relaxation rate drops below T_c , while (e) the quadrupole relaxation rate shows an unconventional coherence peak. (c) The Fermi surface of the s -wave superconducting gap, where the gap is isotropic. (f) The Fermi surface of the d -wave superconducting gap, where the gap changes sign from positive (green) to negative (yellow). The arrow describes the scattering from positive to negative gap value, which leads to a sign change $\Delta_k \Delta_{k+q} < 0$ in the quadrupole relaxation rate coherence factor $C = 1 - \Delta_k \Delta_{k+q} / E_k^2$.

ation rate, as illustrated in Fig. 4 (a), whereas the quadrupole relaxation rate drops below T_c due to coherence factors, as illustrated in Fig. 4 (b). It reflects that the gap is isotropic without a sign reversal in conventional superconductors, as shown in Fig. 4 (c). Conversely, unconventional superconducting gaps exhibit a sign reversal attributed to electron-electron correlation. In such cases, the magnetic relaxation rate does not display a coherence peak around T_c experimentally, and the quadrupole relaxation rate acquires a coherence peak, as illustrated in Figs. 4(d) and 4(e). Historically, the absence of the Hebel-Slichter coherence peak in $1/T_1^{\text{mag}}$ was widely discussed [7–9, 30–34]. One of the prevailing views is that the sign-changing gap is the reason for this absence, which eliminates the coherence factor contribution [17, 30–32]. Meanwhile, it will lead to a phenomenon that the $1/T_1^{\text{quad}}$ be enhanced by the coherence factors just below T_c due to the gap sign changes at various positions around Fermi surfaces, with scattering between different signs becoming dominant, as shown in Fig. 4 (f).

The sharp contrasts observed in $1/T_1^{\text{mag}}$ and $1/T_1^{\text{quad}}$ from conventional superconductors provide a novel method to explore the unconventional nature of the pairing mechanism in unconventional superconductors.

The spin-singlet Cooper pairs are widely believed to be formed above T_c owing to the small superfluid density in unconventional superconductors[35]. The unconventional peak observed in $1/T_1^{\text{quad}}$ leads to a hallmark of forming phase coherent unconventional superconducting condensate below T_c . This peak can be used to diagnose unconventional (sign-changing gap) superconductivity with significant quadrupole relaxation.

On the other hand, measurement conditions for $1/T_1^{\text{quad}}$ are quite stringent, necessitating substantial EFG fluctuations, significant η and the presence of two or more isotopes. Cuprates have charge-density wave (CDW) fluctuations in the phase diagram[36, 37], which provide opportunity to detect $1/T_1^{\text{quad}}$. Although CDW fluctuations contribute to $1/T_1^{\text{quad}}$, the peak found here cannot be due to CDW which competes with superconductivity and CDW order appears only when superconductivity is killed. Some cuprates contain chain Cu with large η and two isotopes $^{63,65}\text{Cu}$. Underdoped $\text{YBa}_2\text{Cu}_3\text{O}_{7-\delta}$ sharing similar electronic band structure with $\text{YBa}_2\text{Cu}_4\text{O}_8$ can also be utilized to identify the unconventional coherence peak[38]. However, measuring $1/T_1^{\text{quad}}$ in other unconventional superconductors poses challenges, such as in iron arsenide where only one iso-

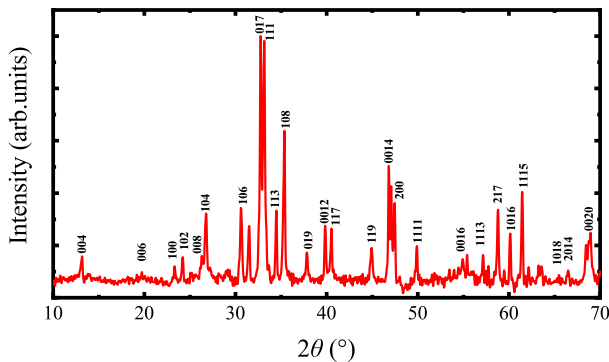


FIG. 5. The x-ray diffraction pattern of $\text{YBa}_2\text{Cu}_4\text{O}_8$ at room temperature.

top of ^{75}As is present[39]. Theoretically, $1/T_1^{\text{quad}}$ can be estimated by comparing the relaxation rate measured by NMR and NQR. However, the different principle axes and the external field make it hard to compare NMR and NQR directly[23]. Another method is to compare the relaxation rate of satellite peaks with the central peak. Nevertheless, achieving this requires exceedingly precise data that surpass current experimental precision levels[20]. As measurement precision improves, there may be opportunities to explore a wider range of systems. We hope our study will inspire extensive future experimental and theoretical investigations to elucidate whether the unconventional coherence peak is a universal characteristic of unconventional superconductivity and delve into its underlying mechanisms.

ACKNOWLEDGMENTS

We thank Professor Chengtian Lin of Max-Planck-Institute für Festkörperforschung for his help in sample synthesis. This work was supported by the National Key Research and Development Program of China (Grants No. 2022YFA1403903, No. 2022YFA1602800, and No. 2022YFA1403901), the National Natural Science Foundation of China (Grants No. 12134018, No. 12174428, No. 11888101, and No. 12488201), the Strategic Priority Research Program and Key Research Program of Frontier Sciences of the Chinese Academy of Sciences (Grant No. XDB33010100), the Chinese Academy of Sciences Project for Young Scientists in Basic Research (2022YSBR-048), the New Cornerstone Investigator Program, and the Synergetic Extreme Condition User Facility (SECUF).

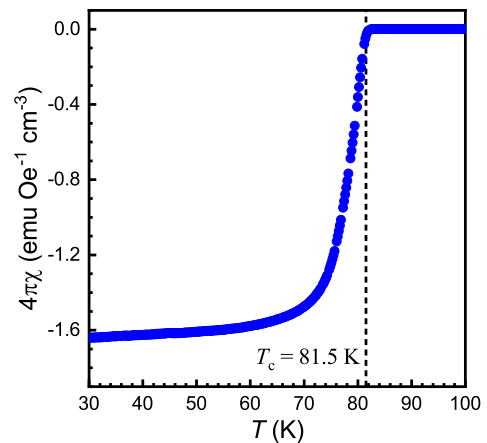


FIG. 6. Temperature-dependent magnetic susceptibility of $\text{YBa}_2\text{Cu}_4\text{O}_8$ single crystal measured at 15 Oe. The data measured with zero field cooling show perfect diamagnetic. The dashed line indicates the superconducting transition temperature.

Appendix A: METHODS

1. Sample growth and characterization

$\text{YBa}_2\text{Cu}_4\text{O}_8$ single crystals are synthesized with $\text{YBa}_2\text{Cu}_3\text{O}_{7-\delta}$ powders and the same molar ratio CuO (99.9%). The precursor $\text{YBa}_2\text{Cu}_3\text{O}_{7-\delta}$ is prepared by solid-state reaction. Stoichiometric proportions of Y_2O_3 (99.99%), BaCO_3 (99.99%), and CuO (99.9%) are thoroughly mixed and grounded and then calcined in air at 860°C for 24 h. The products are ground and then pressed into a pellet and calcined at 890°C for 48 h in $\text{Ar}(95\%)\text{-O}_2(5\%)$. The prepared $\text{YBa}_2\text{Cu}_3\text{O}_{7-\delta}$ powders and CuO are mixed uniformly and then put into the Al_2O_3 crucible with 50 ~ 70 wt% KOH as flux. After keeping at 700°C for 4 h, samples are cooled to 500°C at a speed of $8^\circ\text{C}/\text{h}$ and fast cooled to room temperature finally. By soaking them in ethanol to remove the flux, we get small single crystals with a typical size of 0.1 mm. The x-ray diffraction pattern demonstrates the samples are $\text{YBa}_2\text{Cu}_4\text{O}_8$, as shown in Fig. 5. The magnetic susceptibility measured with a magnetic property measurement system (MPMS-III) exhibits perfect diamagnetism, as shown in Fig. 6.

2. NQR measurements

The skin effect of the metallic state and the penetration depth of the superconducting state can shield the detection signal into the sample, so to achieve a large detectable volume we ground the samples and sieve with 300 mesh standard sieves to ensure a uniform powder particle size ($< 50 \mu\text{m}$). NQR measurements are carried out using a commercial NMR spectrometer from Thamway Co. Ltd. The NQR spectra are acquired by integrating

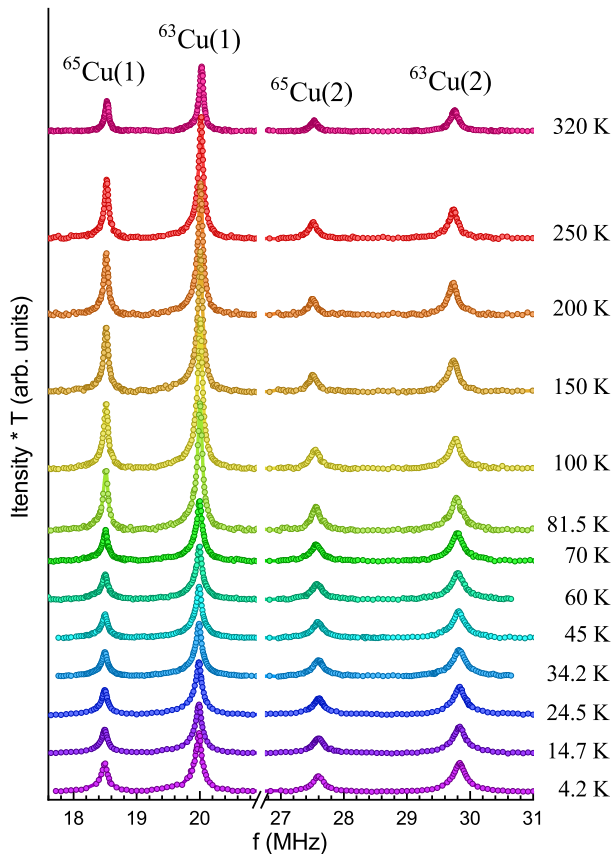


FIG. 7. NQR spectra of $\text{YBa}_2\text{Cu}_4\text{O}_8$ at some typical temperatures. The curves are vertically offset for clarity. Four peaks are $^{65,63}\text{Cu}$ of the Cu(1) site and Cu(2) site, respectively. The nature abundance of ^{63}Cu and ^{65}Cu are 69 % and 31 % respectively, which lead to a peak intensity of ^{63}Cu about twice that of ^{65}Cu .

the intensity of spin echo at each frequency, as shown in Fig. 7. The quadrupole resonance frequencies ν_Q are summarized in Fig. 8. We notice that the ν_Q of Cu(1) shows a small kink at T_c and decreases below T_c in Fig. 8. It is natural to ask whether this kink can influence the spin-lattice relaxation rate R . First of all, the change in ν_Q is equal to the static EFG change crossing T_c . There are two possible origins for this static EFG change: (a) the electronic structure changes; (b) the coupling between electron and nuclear changes. Then, we can separate ν_Q change into two cases:

- If the static EFG change comes from the electrons, the only electronic changes that occur at T_c are from the superconductivity. So, this case is equal to saying that the superconducting ordering induces both the ν_Q change and R peak crossing T_c . And the ν_Q change indicates that superconducting does influence the Cu(1) chain. In this case, R is decided by superconducting transition but not ν_Q .
- If the static EFG change comes from the coupling, we can estimate this change to R . As discussed in

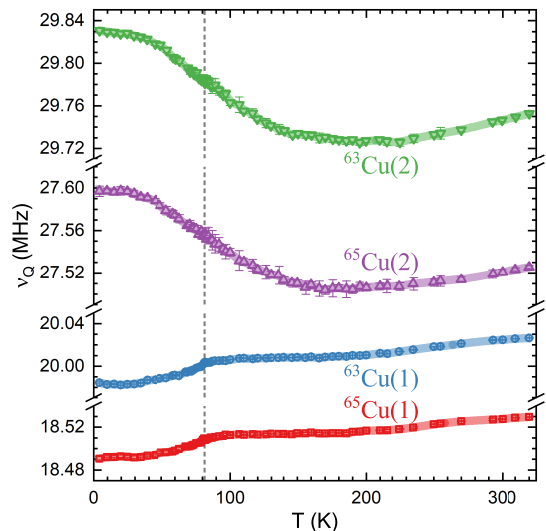


FIG. 8. Temperature-dependent quadrupole resonance frequencies of $^{63,65}\text{Cu}$ of the Cu(1) site and Cu(2) site. T_c is marked with a dashed line. The frequencies change little with temperature over the entire temperature range, even in the superconducting state. The spin-lattice relaxation rate at each temperature is measured at the corresponding frequencies.

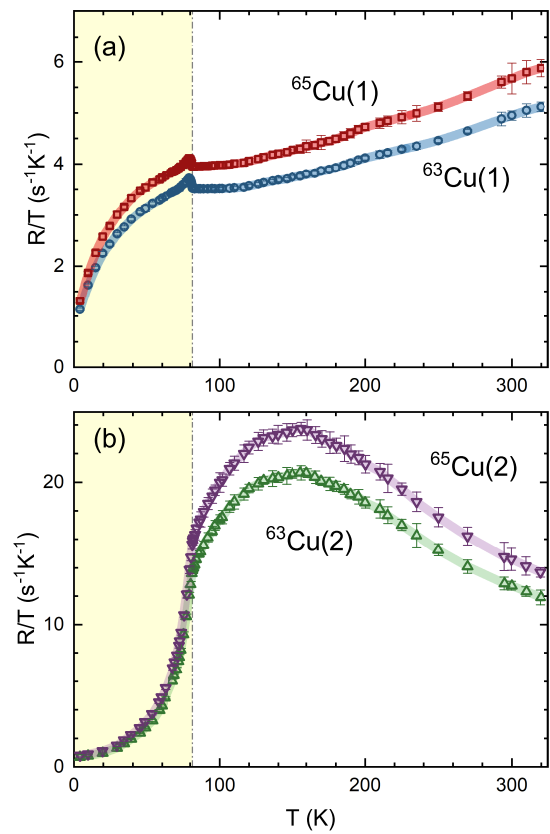


FIG. 9. Temperature-dependent spin-lattice relaxation rates R/T of ^{65}Cu and ^{63}Cu at the Cu(1) site and the Cu(2) site, respectively. The superconducting state is marked in yellow.

the theoretical analysis subsection, the spin relaxation rate is proportional to the relaxation matrix W_{mn} between a state $|m\rangle$ and $|n\rangle$ by $|\langle m|H_Q|n\rangle|^2$. Hence, the static EFG influence to the R by the $(\nu_Q + \delta\nu_Q)^2/\nu_Q^2 \approx 1 + 2\delta\nu_Q/\nu_Q$. In other words, if we imagine the change of R comes from a static coupling change instead of the electron fluctuations, the R by the static EFG is changed by $2\delta\nu_Q/\nu_Q$.

We know that $\delta\nu_Q$ just below T_c is less than 0.03% in Fig. 8. This means 0.03% change of static EFG will change R by 0.06% in case (b). However, the R in Fig. 2 (a) increases about 5% just below T_c which is much larger than this small change. Moreover, ν_Q decreases monotonically with decreasing temperature below T_c , while R peaks just below T_c and decreases at lower temperatures. So the peak of R cannot come from ν_Q change. The change of R reflects the change of DOS and the appearance of the coherence factor in the superconducting state.

Spin-lattice relaxation rate R for every nucleus is measured using a comb-shaped-pulse recovery method with the recovery function $M(t) = M(\infty) - A \exp(-Rt)$, where error bars are the standard error of the least square fit. $M(t)$ is the nuclear magnetization at time t after saturation pulses. $M(\infty)$ is the value of $M(t)$ in an equilibrium state and $A = M(\infty) - M(0)$, where $M(0)$ is the initial value of $M(t)$ after the saturation pulses. Both $M(\infty)$ and A are fitting parameters. R/T in the full temperature zone is shown in Fig. 9. R can be written as a sum of two contributions of $1/T_1^{\text{mag}}$ and $1/T_1^{\text{quad}}$, ${}^{63,65}R = 3/{}^{63,65}T_1^{\text{mag}} + 1/{}^{63,65}T_1^{\text{quad}}$ for ${}^{63,65}\text{Cu}$ NQR experiment. $1/T_1^{\text{mag}}$ is proportional to the square of the gyromagnetic ratio, $1/T_1^{\text{mag}} \propto \gamma^2$, so $a \equiv ({}^{63}T_1^{\text{mag}}/{}^{65}T_1^{\text{mag}}) = ({}^{65}\gamma/{}^{63}\gamma)^2 = 1.1477$. $1/T_1^{\text{quad}}$ is proportional to the square of the quadrupole moment, $1/T_1^{\text{quad}} \propto Q^2$, so $b \equiv ({}^{63}T_1^{\text{quad}}/{}^{65}T_1^{\text{quad}}) = ({}^{65}Q/{}^{63}Q)^2 = 0.8562$. Based on these relationships, $1/T_1^{\text{mag}}$ and $1/T_1^{\text{quad}}$ can be distinguished.

We want to add a note here. The EFG principal axis of Cu(1) is along the a axis and the principal axis of Cu(2) is along the c axis[4]. In a conventional superconductor, the Hebel-Slichter coherence peak appears in all directions. The coherence peak reflects the divergence of DOS and coherence between electrons. Whether there is a coherence peak does not depend on the direction of the principal axes of EFG. However, if one wants to separate $1/T_1^{\text{mag}}$ and $1/T_1^{\text{quad}}$ by comparing NMR and NQR, or by comparing atoms at different sites, the principal axis is important. $1/T_1^{\text{mag}}$ is determined by the fluctuations perpendicular to the applied magnetic field and $1/T_1^{\text{quad}}$ is determined by the fluctuations perpendicular to the principal axes when $\eta = 0$. The mismatch between the applied magnetic field and the principle axes leads to different $1/T_1$ values of NMR from NQR. When $\eta > 0$, even if the applied field is along the principal axes, NMR and NQR cannot get the same $1/T_1$ value[23]. Moreover, the

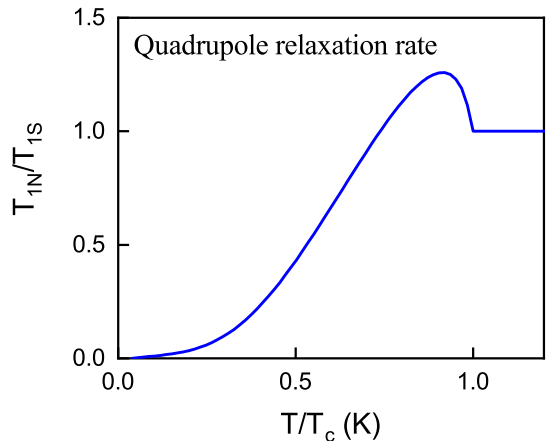


FIG. 10. The theoretical simulation for the quadrupole relaxation rate in d -wave superconductors. Here, we limit the summation around (π, π) .

principal axes of Cu(1) and Cu(2) are different, so their $1/T_1$ from NQR cannot be compared directly[4]. We use the method of comparing $1/T_1$ of ${}^{63}\text{Cu}$ and ${}^{65}\text{Cu}$ at the same site, which have the same EFG and form factor, to avoid this problem.

3. Theoretical analysis

The Hamiltonian of quadrupole interaction can be compactly written as

$$H_Q = eQ \int dr V_{\mu\nu}(r) I_{\mu\nu}(r). \quad (\text{A1})$$

The EFG tensor $V_{\mu\nu}$ can be expressed as $V_{\mu\nu}(r) = \int dr' \rho(r') T_{\mu\nu}(r, r')$ where $T_{\mu\nu}(r, r')$ is the spatial function linking the electron density $\rho(r')$ to nucleus quadrupole $I_{\mu\nu}(r)$. Thus, the charge fluctuation in NQR is mainly determined by the density fluctuation of electrons and quadrupole of the nuclear. The Fourier transformed Hamiltonian in the lattice can be expressed as $H_Q = e \sum_q F(q) \rho(q) A(-q)$, where $F(q)$ is the structure factor determined by $T_{\mu\nu}(r, r')$ and A contains the quadrupole moment and spin of nuclear. The relaxation of the nuclear spin and lattice toward the thermodynamic equilibrium can be described by the master equation $\frac{dP(t)}{dt} = W_{mn} [P(t) - P(0)]$, where $P(t)$ is the population vector of the different energy levels [20]. The relaxation matrix W_{mn} is given by $W_{mn} \propto T \sum_q F^2(q) \lim_{\omega \rightarrow 0} \frac{\text{Im} \chi_{\rho\rho}(q, \omega)}{\omega}$ through second-order perturbation theory. Here $\chi_{\rho\rho}(q, \omega)$ is the density-density correlation function. For superconductors, $\chi_{\rho\rho}(q, \omega)$ can be

calculated by the Green's function as

$$\chi_{\rho\rho}(q, i\omega_n) = F^2(q) \frac{1}{\beta} \sum_{k, i\nu_n} \text{Tr} [G(k, i\nu_n) \tau_3 G(k+q, i\nu_n + i\omega_n) \tau_3], \quad (\text{A2})$$

where τ_3 is the Pauli matrix and $G(k, i\nu_n)$ is the Matsubara Green's function for SC. Then we can get

$$\frac{1}{T_1^{\text{quad}}} \propto -T \sum_{kq} \left(1 - \frac{\Delta_k \Delta_{k+q}}{E_k^2} \right) F^2(q) \frac{\partial f(E_k)}{\partial E_k} \delta(E_k - E_{k+q}) \quad (\text{A3})$$

As we discuss in the main text, the coherence peak is from the CuO₂ plane. By focusing on the plane, Fig. 10 shows the quadrupole relaxation rate in *d*-wave superconductors calculated by summing the q points near (π, π) .

The above analysis provides a qualitative understanding of the coherence peak in *d*-wave superconductors. On the other hand, since NQR relaxation rate can be observed only on the Cu(1) sites rather than on the Cu(2) sites due to a nonzero η on CuO chains, we need consider a multiband model including both CuO planes and CuO chains to more convincingly describe the experimental phenomena. The Hamiltonian of the two-band model can be written as

$$H_0 = \sum_{nk} \varepsilon_{nk} c_{nk\sigma}^\dagger c_{nk\sigma} + \varepsilon_{\perp k} \left(c_{1k\sigma}^\dagger c_{2k\sigma} + \text{H.c.} \right) + \sum_{nk} \Delta_n \phi_{nk} \left(c_{nk\uparrow}^\dagger c_{n-k\downarrow}^\dagger + \text{H.c.} \right). \quad (\text{A4})$$

The dispersions of the CuO chain ($n = 1$) and CuO plane ($n = 2$) are $\varepsilon_{1k} = -2t_{cNN} \cos k_x + \varepsilon_c$ and $\varepsilon_{2k} = -2t_{pNN} (\cos k_x + \cos k_y) + 4t_{pNNN} \cos k_x \cos k_y + \varepsilon_p$ respectively. The tunneling term between the two layers has the form $\varepsilon_{\perp k} = t_{cp} + 2t_{cpNN} (\cos k_x - \cos k_y)$. All the parameters in the tight-binding model can be obtained from the density-functional theory calculations. $\Delta_n \phi_{nk}$ is the mean-field order parameter of the chain and plane bands. To our knowledge, how the chain becomes superconducting remains controversial. Since the failure of considering only the single-particle tunneling model has been highlighted in Ref. [25], we take the pair tunneling interaction, specifically Josephson coupling. The singlet pair tunneling term has the form

$$H_I = -\lambda_J \sum_{kk'} \left(\phi_{1k} \phi_{2k'} c_{1k\uparrow}^\dagger c_{1-k\downarrow}^\dagger c_{2-k'\downarrow} c_{2k'\uparrow} + \text{H.c.} \right), \quad (\text{A5})$$

where λ_J is the Josephson coupling strength. Because of symmetry requirements, Josephson coupling imposes the same pairing symmetry on both the CuO chains and

planes. Thus, we set $\phi_{1k} = \phi_{2k} = \cos k_x - \cos k_y$. Then

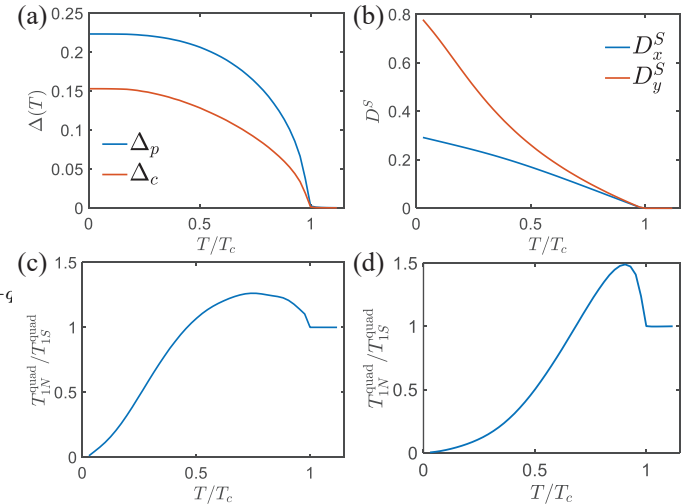


FIG. 11. (a) The amplitude of order parameters on CuO chain Δ_c and plane Δ_p through the self-consistent calculation. (b) The superfluid density along x and y directions. (c) The quadrupole relaxation rate on the CuO chain [Cu(1) site]. (d) The quadrupole relaxation rate on the CuO plane [Cu(2) site]. The parameters in calculation are set as $t_{pNN} = 0.36$, $t_{pNNN} = 0.12$, $t_{cNN} = 0.45$, $t_{cp} = 0.014$, $t_{cpNN} = 0.04$, $\varepsilon_c = 0.26$, $\varepsilon_p = 0.22$, $\lambda_1 = \lambda_2 = 0.8$ and $\lambda_J = 0.15$.

Δ_n can be determined by self-consistent equations

$$\Delta_1 = \frac{\lambda_1}{V} \sum_k \phi_{1k} \langle c_{1k\uparrow} c_{1-k\downarrow} \rangle + \frac{\lambda_J}{V} \sum_k \phi_{2k} \langle c_{2k\uparrow} c_{2-k\downarrow} \rangle, \quad (\text{A6})$$

$$\Delta_2 = \frac{\lambda_J}{V} \sum_k \phi_{1k} \langle c_{1k\uparrow} c_{1-k\downarrow} \rangle + \frac{\lambda_2}{V} \sum_k \phi_{2k} \langle c_{2k\uparrow} c_{2-k\downarrow} \rangle,$$

where λ_n are strengths of intralayer pairing potentials. Figure 11(a) shows the amplitude of order parameters on the CuO chain and plane. Because of Josephson coupling, the order parameter from the CuO planes penetrates into the chains. As a result, the phase coherence properties of the planes can also be detected in the chains. Note that if $\lambda_J = 0$, the self-consistent calculation will yield a very small value for Δ_c . Furthermore, we calculate the superfluid density along x and y directions shown in Fig.11(b). The quadrupole relaxation rate projected on the chain and plane bands can be calculated using this two-band model. Figure 11(c) and 11(d) show the results. The quadrupole relaxation rate on the CuO chain qualitatively captures the main features in the experiment: The coherence peak occurs just below T_c . We emphasize that the conclusions do not depend on the specific form of interlayer coupling, as we also achieve the similar results using the single-particle tunneling model.

[1] L. Taillefer, Scattering and pairing in cuprate superconductors, in *Annual Review of Condensed Matter Physics*,

- Vol. 1, edited by J. S. Langer (2010) pp. 51–70.
- [2] T. Imai, T. Shimizu, T. Tsuda, H. Yasuoka, T. Takabatake, Y. Nakazawa, and M. Ishikawa, Nuclear Spin-Lattice Relaxation of $^{63,65}\text{Cu}$ at the Cu(2) Sites of the High T_c Superconductor $\text{YBa}_2\text{Cu}_3\text{O}_{7-\delta}$, *Journal of the Physical Society of Japan* **57**, 1771 (1988).
 - [3] T. Imai, T. Shimizu, H. Yasuoka, Y. Ueda, and K. Kosuge, Anomalous Temperature Dependence of Cu Nuclear Spin-Lattice Relaxation in $\text{YBa}_2\text{Cu}_3\text{O}_{6.91}$, *Journal of the Physical Society of Japan* **57**, 2280 (1988).
 - [4] H. Zimmermann, M. Mali, D. Brinkmann, J. Karpinski, E. Kaldis, and S. Rusiecki, Copper NQR and NMR in the superconductor $\text{YBa}_2\text{Cu}_4\text{O}_{8+x}$, *Physica C: Superconductivity* **159**, 681 (1989).
 - [5] W. W. Warren and R. E. Walstedt, NQR and NMR Studies of Spin Dynamics in High T_c Superconducting Cuprates, *Zeitschrift für Naturforschung A* **45**, 385 (1990).
 - [6] T. Machi, I. Tomeno, T. Miyatake, N. Koshizuka, S. Tanaka, T. Imai, and H. Yasuoka, Nuclear spin-lattice relaxation and Knight shift in $\text{YBa}_2\text{Cu}_4\text{O}_8$, *Physica C: Superconductivity* **173**, 32 (1991).
 - [7] K. Asayama, Y. Kitaoka, G.-q. Zheng, and K. Ishida, NMR studies of high T_c superconductors, *Progress in Nuclear Magnetic Resonance Spectroscopy* **28**, 221 (1996).
 - [8] T. Imai, C. P. Slichter, J. L. Cobb, and J. T. Markert, Superconductivity and spin fluctuations in the electron-doped infinitely-layered high T_c superconductor $\text{Sr}_{0.9}\text{La}_{0.1}\text{CuO}_2$ ($T_c = 42$ K), *Journal of Physics and Chemistry of Solids* **56**, 1921 (1995).
 - [9] A. Rigamonti, F. Borsa, and P. Carretta, Basic aspects and main results of nmr-nqr spectroscopies in high-temperature superconductors, *Reports on Progress in Physics* **61**, 1367 (1998).
 - [10] M. Jurkutat, M. Avramovska, G. V. M. Williams, D. Dernbach, D. Pavicevic, and J. Haase, Phenomenology of ^{63}Cu Nuclear Relaxation in Cuprate Superconductors, *Journal of Superconductivity and Novel Magnetism* **32**, 3369 (2019).
 - [11] L. C. Hebel, Theory of Nuclear Spin Relaxation in Superconductors, *Physical Review* **116**, 79 (1959).
 - [12] C. P. Slichter, *Principles of Magnetic Resonance*, Springer Series in Solid-State Sciences (Springer Berlin Heidelberg, 1990).
 - [13] C. P. Slichter, Magnetic resonance studies of high temperature superconductors, in *Handbook of High-Temperature Superconductivity: Theory and Experiment*, edited by J. R. Schrieffer and J. S. Brooks (Springer New York, New York, NY, 2007) pp. 215–256.
 - [14] D. E. MacLaughlin, Magnetic resonance in the superconducting state, in *Solid State Physics*, Vol. 31, edited by F. S. Henry Ehrenreich and T. David (Academic Press, 1976) pp. 1–69.
 - [15] S. Wada and K. Asayama, Nuclear Quadrupole Spin-Lattice Relaxation of Ta^{181} in Type II Superconducting Ta_3Sn , *Journal of the Physical Society of Japan* **34**, 1168 (1973).
 - [16] Z. Li, W. H. Jiao, G. H. Cao, and G.-q. Zheng, Charge fluctuations and nodeless superconductivity in quasi-one-dimensional $\text{Ta}_4\text{Pd}_3\text{Te}_{16}$ revealed by ^{125}Te -NMR and ^{181}Ta -NQR, *Phys. Rev. B* **94**, 174511 (2016).
 - [17] T. Xiang and C. Wu, *D-wave Superconductivity* (Cambridge University Press, Cambridge, 2022).
 - [18] J. Karpinski, E. Kaldis, E. Jilek, S. Rusiecki, and B. Bucher, Bulk synthesis of the 81-K superconductor $\text{YBa}_2\text{Cu}_4\text{O}_8$ at high oxygen pressure, *Nature* **336**, 660 (1988).
 - [19] F. Raffa, T. Ohno, M. Mali, J. Roos, D. Brinkmann, K. Conder, and M. Eremin, Isotope Dependence of the Spin Gap in $\text{YBa}_2\text{Cu}_4\text{O}_8$ as Determined by Cu NQR Relaxation, *Physical Review Letters* **81**, 5912 (1998).
 - [20] A. Suter, M. Mali, J. Roos, and D. Brinkmann, Mixed magnetic and quadrupolar relaxation in the presence of a dominant static Zeeman Hamiltonian, *Journal of Physics-Condensed Matter* **10**, 5977 (1998).
 - [21] I. Mangelschots, M. Mali, J. Roos, D. Brinkmann, S. Rusiecki, J. Karpinski, and E. Kaldis, ^{17}O NMR study in aligned $\text{YBa}_2\text{Cu}_4\text{O}_8$ powder, *Physica C: Superconductivity* **194**, 277 (1992).
 - [22] A. Suter, M. Mali, J. Roos, and D. Brinkmann, Charge degree of freedom and the single-spin fluid model in $\text{YBa}_2\text{Cu}_4\text{O}_8$, *Physical Review Letters* **84**, 4938 (2000).
 - [23] A. Goto, T. Shimizu, H. Aoki, M. Kato, K. Yoshimura, K. Kosuge, T. Matsumoto, and Y. Yamada, Anisotropy Study of the Spin-Lattice Relaxation Rates at the Cu(1) Chain Sites of $\text{YBa}_2\text{Cu}_3\text{O}_7$ and $\text{YBa}_2\text{Cu}_4\text{O}_8$, *Journal of the Physical Society of Japan* **67**, 759 (1998).
 - [24] F. Raffa, M. Mali, A. Suter, A. Y. Zavidonov, J. Roos, D. Brinkmann, and K. Conder, Spin and charge dynamics in the Cu-O chains of $\text{YBa}_2\text{Cu}_4\text{O}_8$, *Physical Review B* **60**, 3636 (1999).
 - [25] T. Xiang and J. M. Wheatley, Superfluid Anisotropy in YBCO: Evidence for Pair Tunneling Superconductivity, *Physical Review Letters* **76**, 134 (1996).
 - [26] A. Serafin, J. D. Fletcher, S. Adachi, N. E. Hussey, and A. Carrington, Destruction of chain superconductivity in $\text{YBa}_2\text{Cu}_4\text{O}_8$ in a weak magnetic field, *Physical Review B* **82**, 140506 (2010).
 - [27] W. A. Atkinson and J. P. Carbotte, Effect of proximity coupling of chains and planes on the penetration-depth anisotropy in $\text{YBa}_2\text{Cu}_3\text{O}_7$, *Physical Review B* **52**, 10601 (1995).
 - [28] R. Gagnon, S. Pu, B. Ellman, and L. Taillefer, Anisotropy of Heat Conduction in $\text{YBa}_2\text{Cu}_3\text{O}_{6.9}$: A Probe of Chain Superconductivity, *Physical Review Letters* **78**, 1976 (1997).
 - [29] H. F. Fong, B. Keimer, P. W. Anderson, D. Reznik, F. Doğan, and I. A. Aksay, Phonon and Magnetic Neutron Scattering at 41 meV in $\text{YBa}_2\text{Cu}_3\text{O}_7$, *Physical Review Letters* **75**, 316 (1995).
 - [30] T. Koyama and M. Tachiki, Theory of nuclear relaxation in superconducting high- T_c oxides, *Phys. Rev. B* **39**, 2279 (1989).
 - [31] H. Monien and D. Pines, Spin excitations and pairing gaps in the superconducting state of $\text{YBa}_2\text{Cu}_3\text{O}_{7-\delta}$, *Phys. Rev. B* **41**, 6297 (1990).
 - [32] D. Thelen, D. Pines, and J. P. Lu, Evidence for $d_{x^2-y^2}$ pairing from nuclear-magnetic-resonance experiments in the superconducting state of $\text{YBa}_2\text{Cu}_3\text{O}_7$, *Phys. Rev. B* **47**, 9151 (1993).
 - [33] M. Zoli, Smearing of the Hebel-Slichter Peak by 2D Fluctuations in Layered Cuprate Superconductors, *Journal of the Physical Society of Japan* **60**, 3837 (1991).
 - [34] B. W. Statt, Anisotropic gap and quasiparticle-damping effects on NMR measurements of high-temperature superconductors, *Physical Review B* **42**, 6805 (1990).
 - [35] V. J. Emery and S. A. Kivelson, Importance of phase fluctuations in superconductors with small superfluid den-

- sity, *Nature* **374**, 434 (1995).
- [36] B. Keimer, S. A. Kivelson, M. R. Norman, S. Uchida, and J. Zaanen, From quantum matter to high-temperature superconductivity in copper oxides, *Nature* **518**, 179 (2015).
- [37] T. Wu, H. Mayaffre, S. Kramer, M. Horvatic, C. Berthier, W. N. Hardy, R. X. Liang, D. A. Bonn, and M. H. Julien, Magnetic-field-induced charge-stripe order in the high-temperature superconductor $\text{YBa}_2\text{Cu}_3\text{O}_y$, *Nature* **477**, 191 (2011).
- [38] T. Oguchi, T. Sasaki, and K. Terakura, Electronic band structure of $\text{YBa}_2\text{Cu}_4\text{O}_8$, *Physica C: Superconductivity* **172**, 277 (1990).
- [39] Z. Li, D. L. Sun, C. T. Lin, Y. H. Su, J. P. Hu, and G. Q. Zheng, Nodeless energy gaps of single-crystalline $\text{Ba}_{0.68}\text{K}_{0.32}\text{Fe}_2\text{As}_2$ as seen via ^{75}As NMR, *Physical Review B* **83**, 140506 (2011).